Nano Express

Preparation and characterization of Ag-nanostars@Au-nanowires hierarchical nanostructures for highly sensitive surface enhanced Raman spectroscopy

To cite this article before publication: Maria Sole Zalaffi *et al* 2020 *Nano Ex.* in press https://doi.org/10.1088/2632-959X/aba104

Article type: Full Paper

Preparation and characterization of Ag-nanostars@Au-nanowires hierarchical nanostructures for highly sensitive surface enhanced Raman spectroscopy

Maria Sole Zalaffi[1], *Lucio Litti*[2], *Patrizia Canton* [1,3], *Moreno Meneghetti*[2], *Ligia Maria Moretto*[1] *and Paolo Ugo*[1]*

1) Department of Molecular Sciences and Nanosystems, University Ca' Foscari of Venice, Via Torino 155, 30170, Venezia Mestre, Italy
2) Department of Chemical Sciences, University of Padova, Via Marzolo 1, 35131, Padova, Italy
3) Department of Molecular Sciences and Nanosystems, University Ca' Foscari of Venice & Electronic Microscopy Center "Giovanni Stevanato", via Torino 155, 30172 Mestre, Italy

*Corresponding author: email ugo@unive.it

Abstract

In this work we study the surface enhanced Raman scattering (SERS) produced by hierarchical nanostructures obtained by coupling different anisotropic nanomaterial of two SERS active metals, namely Ag nanostars (AgNSs) and Au nanowires (AuNWs). Ag nanostars (AgNSs) are prepared, by a two-step one-pot synthesis by reduction of $AgNO_3$ with hydroxylamine, trisodium citrate and NaOH. AuNWs are obtained by electroless templated synthesis in track-etched polycarbonate membranes with following etching of the template. The two precursors are bound together by bridging with the bifunctional thiol cysteamine, obtaining AgNS@AuNW hierarchical structures. Benzenethiol (BT) is adsorbed on the nanostructured material and used as SERS probe to study the amplification of Raman signals. Experimental results indicate significantly larger Raman enhancement when BT is adsorbed onto the AgNS@AuNW in comparison to AuNWs alone or decorated with quasi-spherical silver nanoparticles obtaining AgNP@AuNW. Digital simulations performed by the boundary element method agree with the experimental findings, showing higher number of hot spots and significantly higher SERS enhancements for AgNS@AuNW vs. AuNWs or AgNSs or AgNP@AuNW.

Keywords: SERS, hierarchical nanostructures, Ag nanostars, Au nanowires, boundary element method

1. Introduction

Ultrasensitive detection of Raman-active molecules is increasingly studied with focus on the development of chemical sensors which exploit the surface enhanced Raman spectroscopy (SERS) [1,2]. Many research efforts are directed towards the development of highly sensitive SERS substrates based on metal nanostructures [3,4], in some cases, hierarchically organized [5-7]. In particular, it was observed that the Raman enhancement generated by spherical nanoparticles (NPs) can be improved using nanomaterials with different shape, especially nanostructures characterized by anisotropic features [8,9]. For instance, large SERS enhancements have been observed using gold sphere segment void nanostructures [10,11] or arrays of macroporous nanostructures produced on bundles of optical fibers [12]. Very high amplification effects have been observed with anistropic nanoparticles such as silver nanoflowers [13,14] and star-shaped NPs, including gold [15,16] or silver nanostars [17] (AgNSs). AgNSs appear particularly attractive since they produce important SERS effects and can be easily synthesized using quite simple one-pot chemical procedures [18]. Because of their starry shape composed of a central core and many pods, these nanoparticles show interaction with UV-Vis-NIR light in particular in two spectral regions, namely in the UV and in the NIR. These factors favor a strong enhancement of the Raman scattering [19,20].

Large SERS effects have been observed for hierarchically organized nanostructures such as AgNPs on vertically aligned semiconductor nanorods [21], or on flat gold [22], starry-shaped AuNPs arrays on Ag films [5], AgNPs assembled on powdered copper substrates [23]. Ag nanocubes on micropyramids of silver functionalized with 4-methylbenzenethiol SERS probe [24]. Positive SERS effects have been generated using Ag:Au bimetallic nanostructures such as SERS active nanosphere arrays composed by Ag underlayer and Au overlayer [25] or Au:Ag bimetallic structures [26].

On the other hand, also nanowire (NW) based structures display significant SERS effects [27-30]. This was demonstrated for silver nanowires [31-33], Au-Ag nanowires [34] and Au-Ag alloy nanotubes decorated with Au nanoparticles [35].

On these bases, in the present work we examine the preparation and application of SERS substrates obtained by combining synergistically the properties of AgNSs and AuNWs to prepare hierarchical nanostructures, here named AgNS@AuNW. The two precursor nanomaterials are prepared separately, by using hard template [36,37] and soft template [18] synthesis for AuNWs and AgNSs, respectively. They are assembled together in the hierarchical structures by cysteamine bridges [38,39]. After careful characterization of the obtained nanostructures by spectroscopic and electron microscopy techniques, the SERS amplification potentialities of AgNS@AuNW are tested with respect to the detection benzenethiol (BT), used as a reference Raman probe. The SERS effectiveness of AgNS@AuNW is evaluated experimentally by comparing the Raman spectra recorded for BT adsorbed onto AgNS@AuNW vs. AuNWs with or without decoration with isotropic silver nanoparticles (AgNPs). Experimental results are discussed and interpreted using digital simulations performed using the boundary element method [40,41] which show that higher number of hot spots and significantly higher SERS enhancements characterize AgNS@AuNW structures vs. AuNWs and AgNP@AuNW.

Experimental

2.1 Chemicals and Materials

All the chemicals used were analytical grade and purchased from Merck-Sigma-Aldrich. Polycarbonate filter membranes, coated by the producer with the wetting agent polyvinylpyrrolidone, were supplied by SPI-Pore Filter (47 mm filter diameter, filter thickness 6 μm, 80 nm pore size, $6x10^8$ pores/cm^{-2} pore density). Double distilled water was used to prepare all the solutions.

2.2 Synthesis of Ag nanostars (AgNSs)

AgNSs were synthesized using the method of A. García-Leis *et al.* [18]. Briefly, 500 μL of 0.05 M NaOH solution and 500 μL of the hydroxylamine solution (18 μL of NH_2OH at 50% w/v in 5 mL of milliQ water) are mixed in a flask and stirred for one minute (magnetic stirrer at 670 rpm). Afterwards, 9 mL of the 10-3 M AgNO3 solution are added and stirred for 5 minutes. Finally, 100 μL of 0.045 M trisodium citrate solution are dropped in the flask, stirring for approximately 15 minutes, i.e. up to a dark green color is developed. The completion of the growth of the AgNSs is performed by storage of the reaction vessel, without stirring in the dark for 48 h at room temperature. The final dispersion is characterized by a green color. TEM analyses performed by us indicate that the appearance of a grey-beige color is indicative of the unsuccessful preparation of a polydisperse system composed both of AgNSs and spherical AgNPs.

2.3 Synthesis of Ag nanospheres (AgNPs)

AgNPs were synthesized adapting the method described in the literature [42,43]. Briefly, $1 \cdot 10^{-3}$ M $AgNO_3$ solution is heated up to boiling then, 1 mL of 0.045 M trisodium citrate solution is added and the mixture is kept under reflux at around 100 °C for one hour. During this procedure, a colloidal dispersion is formed, assuming a matt appearance and a light beige color.

2.4 Membrane template preparation of Au nanowires (AuNWs)

Ensembles of gold nanowires embedded in the polycarbonate (PC) template (2DNEEs) were prepared by the electroless membrane template procedure described previously [44-46]. Briefly, after dipping the PC membrane in methanol for 4 h, it was sensitized with Sn^{2+} in a solution containing 0.026 mol L^{-1} $SnCl_2$ and 0.07 mol L^{-1} trifluoroacetic acid in 50:50 methanol:water for 45 min. After rinsing with methanol, the membrane was dipped in 0.026 mol L^{-1} $Ag[(NH_3)_2]NO_3$ for 10 min. Successively, it was immersed in an Au plating bath containing 7.9×10^{-3} mol L^{-1} $Na_3Au(SO_3)_2$ in 0.127 mol L^{-1} Na_2SO_4 at 0 °C. After 20 min, 0.625 mol L^{-1} formaldehyde was

added to the solution. Electroless deposition was allowed to proceed for 24 hours. After this period the golden membrane was washed with water and immersed in 10% HNO_3 solution for 12 hours. At the end of the electroless deposition, gold is deposited both within the pores and the outer faces of the membrane. Therefore, to expose the polycarbonate, the outer gold layer was removed from one face of the membrane by peeling with scotch tape (Scotch® Magic™ by 3M). In order to remove the polycarbonate of the templating membrane to expose the AuNWs, two different etching processes were applied, one to perform the partial and the other for the total etching. For the partial etching, the AuNWs, 2DNEEs were dipped for 30 s in CH_2Cl_2:EtOH 1:9 [45]. The total etching of the polycarbonate [47], was instead achieved by attaching a 2DNEE onto a Teflon support by means of Kapton adhesive tape and pouring pure dichloromethane several times on the tilted sample. Exposed AuNWs were cleaned by residues of PC by using a procedure recently described [48], based on the use of a cold atmospheric plasma jet system, namely, Stylus Plasma Noble produced by NADIR SrL (Italy). For the present application, the following parameters were employed: Ar/O_2 flux= 8 L/min; t= 60 s; HV= 4 W – Gain 40%; RF= 15 W pulsed; WD= 8 mm.

2.5 Preparation of the samples for the Raman analysis

The macro-gold slides and the AuNWs arrays employed for the benzenethiol (BT) detection were prepared as follows:

1. overnight immersion in 10 mM cysteamine solution in water;
2. overnight immersion in the colloidal suspension of nanoparticles (AgNPs or AgNSs);
3. overnight immersion in 10^{-5} M BT solution in ethanol.

Careful washing with water was performed between the above steps. The obtained hierarchical structures resulted stable. It was observed that omitting step 1, the AgNPs and AgNSs that initially adhered to the AuNWs, were removed by washing with water or ethanol.

2.6 Instrumentation

2.6.1 SERS and Raman Spectroscopy

The Raman spectra were recorded using a Renishaw inVia Raman spectrometer equipped with a diode laser operating at 785 nm (300 mW max power), used at 0.1% of its power, with an acquisition time of 10 s, coupled with an optical microscope (Leica), with objective 20X/0.4. The post-processing of the spectra was performed with the OriginLab software. Because of some inhomogeneity of the examined samples, as usual for deposited samples, preliminary measurements were performed analyzing different areas. And the spectra reported and compared in this work are those with the highest signals.

2.6.2 UV-Visible-NIR Absorption Spectroscopy

UV-Vis absorbance spectra were recorded with a Perkin-Elmer Lambda 40 spectrophotometer equipped with a Peltier-Elmer PTP6 (Peltier temperature programmer) apparatus. The samples were diluted 1:3 in water as regards the Ag colloids and in dichloromethane for AuNWs suspensions.

2.6.3 Electron Microscopy

A JEOL 3010 high resolution electron microscope (0.17 nm point-to-point resolution at Scherzer defocus), operating at 300 kV, equipped with a Gatan slow-scan CCD camera (model 794) was used for transmission electron microscopy (TEM). Drops of colloidal solutions were deposited on Holey-Carbon Copper grids and let dry at room temperature before analysis.

Field-emission scanning electron microscopy (FE-SEM) analysis were performed using a Sigma-VP Carl Zeiss electron microscope. Solid samples were immobilized on stubs by means of conductive tape in order to prevent charging effects.

2.6.4 Dynamic Light Scattering (DLS)

DLS measurements were performed at room temperature with a Zetasizer Nano ZS (Malvern Instruments) equipped with a green laser (λ = 532 nm) and backscatter detector at 175°.

2.6.5 Boundary Element Method (BEM) simulations

The digital structures used to simulate the nanomaterials in this study were produced by a 3D design modeling software (Blender 2.79b) and then imported in Matlab environment. The minimum distance between Ag star and Au NW was fixed at 0.5 nm, as it is reported to be the minimum distance avoiding complex coupling effects [49]. The attribution of the physical properties for the nanostructures and the environments, as well the spectra and local fields simulations, were done using the MNPBEM libraries developed by U. Hohenester *et al*. [40,41]. The exciting fields (with excitation source at 785 nm) are considered as propagating along the x, y and z axes and polarized along the two other normal directions for each case. The results are an average of the different field excitations, simulating the situation of a nanostructure at a random orientation with respect of the incoming field. The Enhancement Factors are calculated as the forth power of the local fields calculated at the surface of the simulated structures, given unitary the intensity of the exciting electromagnetic field. This can be done because the frequency of the exciting light and that of the scattered light are very similar, being the difference that of a vibrational frequency.

3. Results and discussion

3.1 Characterization of AgNSs, AgNPs, AuNWs precursors

The different nanomaterials used here as precursors for the preparation of the desired hierarchical nanostructures have been synthesized using known procedures (see Experimental), however in order to obtain specifically the morphological and physicochemical information required for this study, they are carefully characterized in view of the achievement of the present purposes.

Figure 1-A and 1-C show the typical TEM images of an individual AgNSs (A) and a group of numerous AgNSs (C), synthesized at pH 8.1. These nanoparticles are characterized by a central core of approximately 50 nm diameter and a variable number of pods arranged in an octahedral structure, reaching an overall dimension of approximately 200 nm. The growth of the anisotropic particle starts from spherical seeds of Ag generated by initial reduction with hydroxylamine, then, in the following 48 hours, the pods grow, being directed by the presence of citrate ions [18] and NaOH [50]. For the sake of comparison, Figure 1-B shows the TEM image of a typical AgNP synthesized as described in the experimental section, which displays a quasi-spherical shape with a diameter of approximately 70 nm. Figures 1-C-D support the critical role of an accurate control of the pH for the correct growth of AgNSs; it shows that operating at pH > 8.1 (e.g. pH= 11.4), a mixture of AgNSs + AgNPs is indeed obtained, as discussed previously in the literature [18].

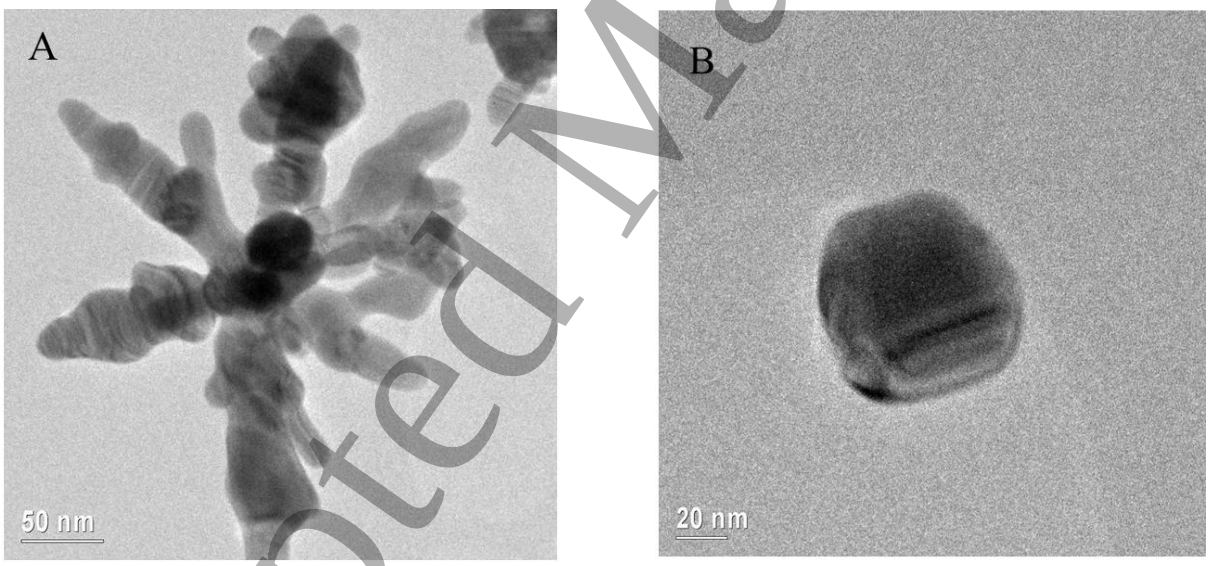

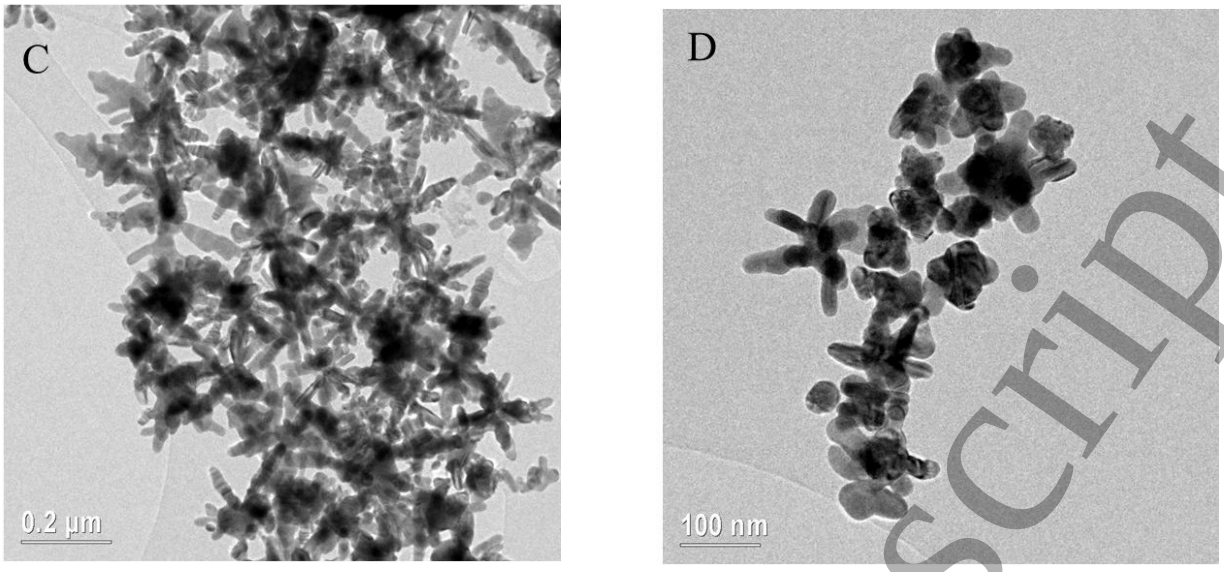

Figure 1 TEM images of : A) individual AgNS; B) individual AgNP; TEM images of colloids obtained: at C) pH 8.1; D) pH 11.4, showing respectively, a monodisperse system formed only of AgNSs and a polydisperse system containing both AgNSs and AgNPs.

In Figure 2, the UV-Vis-NIR extinction spectrum UV-Vis-NIR of a colloidal suspension of AgNSs is reported and compared with the spectrum of a suspension of AgNPs. The comparison shows that Ag nanospheres present maximum extinction at ≈ 430 nm [43], followed by a marked decrease up to reaching zero at $\lambda > 800$ nm. The AgNSs present an extinction maximum at 370 nm, however with further absorption extended throughout the NIR region, up to reaching values comparable with the first maximum at 370 nm.

These features agree with the particular shape of the nanostars [18]: the extinction at 370 nm is caused by the central core while the several pods produce the broad absorption band in the NIR region at $\lambda > 780$ nm. This extinction is influenced by the number and the geometry of the pods and it can even generate a sharp band in some cases [15].

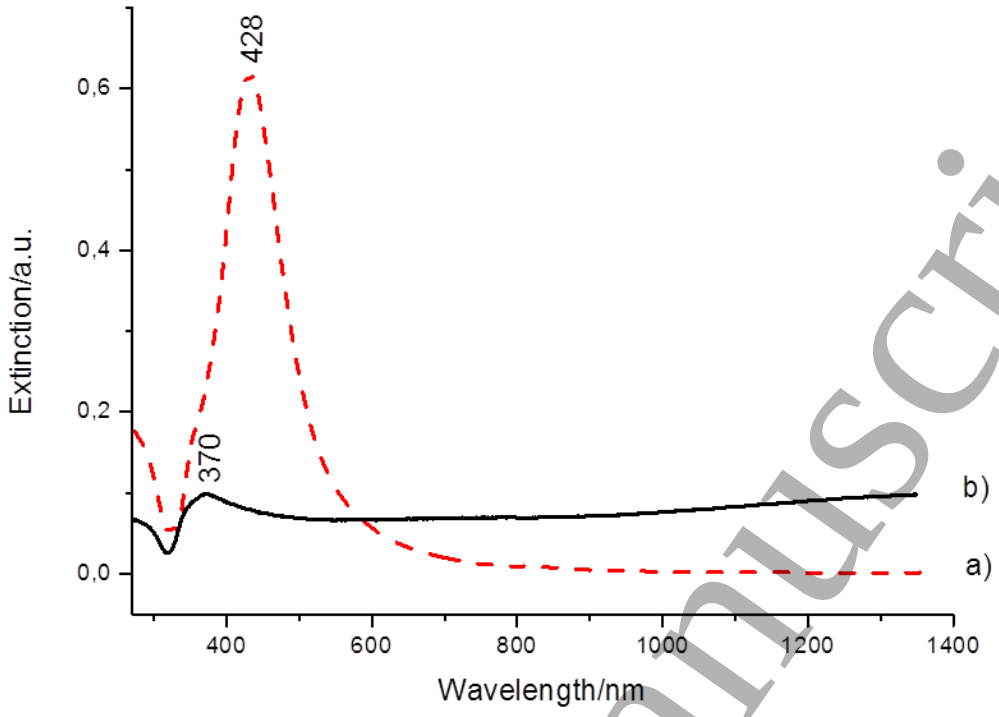

Figure 2 UV-Vis-NIR extinction spectra of colloidal dispersion of the a) AgNPs and b) AgNSs here synthesized.

The average size and polydispersity are evaluated by dynamic light scattering (DLS) measurements [51]. Data reported in Figure 3, indicate an average diameter of 200 nm for the AgNSs (Figure 3-a) and 70 nm for the AgNPs. The polydispersity index (PdI) presents a lower value for the nanospheres (0.258) and a higher value for the nanostars (0.504). Both AgNSs and AgNPs exhibit a negative zeta potential, -44 and -33 mV respectively, which can be attributed to the presence of residual citrate. Both the obtained colloidal dispersions of AgNPs and AgNSs, are stable and do not tend to aggregate.

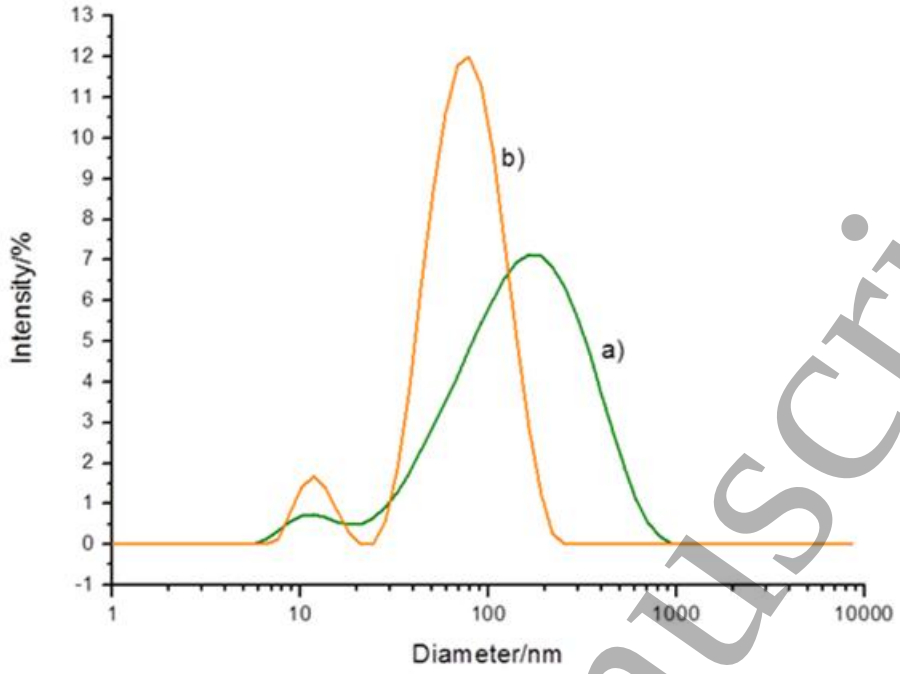

Figure 3 Dynamic light scattering experimental results presenting the size distribution by intensity of a) AgNSs and b) AgNPs.

3.2 Characterization of the AuNWs by UV-Vis-NIR spectroscopy and FE-SEM

Figure 4-A presents the typical extinction spectrum of AuNWs dispersed in dichloromethane, which is characterized by a maximum at λ= 532 nm, in agreement with previous literature findings for similar nanomaterials [52]. Figure S1 in the Supporting Materials (SM) schematizes the morphology of the ensembles of AuNWs at different steps of their preparation [44-46]. Figure 4-B shows the surface of a 2DNEE after peeling the outer gold layer, with the nanowires still inside the membrane pores. Finally, Figure 4-C presents the AuNWs completely exposed after abundant washing with CH_2Cl_2. Eventual traces of residual polycarbonate of the template were removed by using a cold atmospheric plasma jet system [48]. The obtained nanowires results approximately 6 µm long, that is the thickness of the templating membrane. The AuNWs are not perfectly cylindrical, instead, they tend to assume a cigar-like shape, with a maximum diameter around 120-150 nm, since they adapt to the cigar-like shape of the track-etched pores in polycarbonate

membranes [45], The high enlargement FE-SEM image in Figure 4-C confirms what discussed in previous studies [46], i.e. that the templated electroless deposition of gold in track-etched membranes starts with the formation of small Au nuclei formed in the inner wall of each nanopore, these nuclei successively growing under the shape of a nanowire formed by stacked nanospheres.

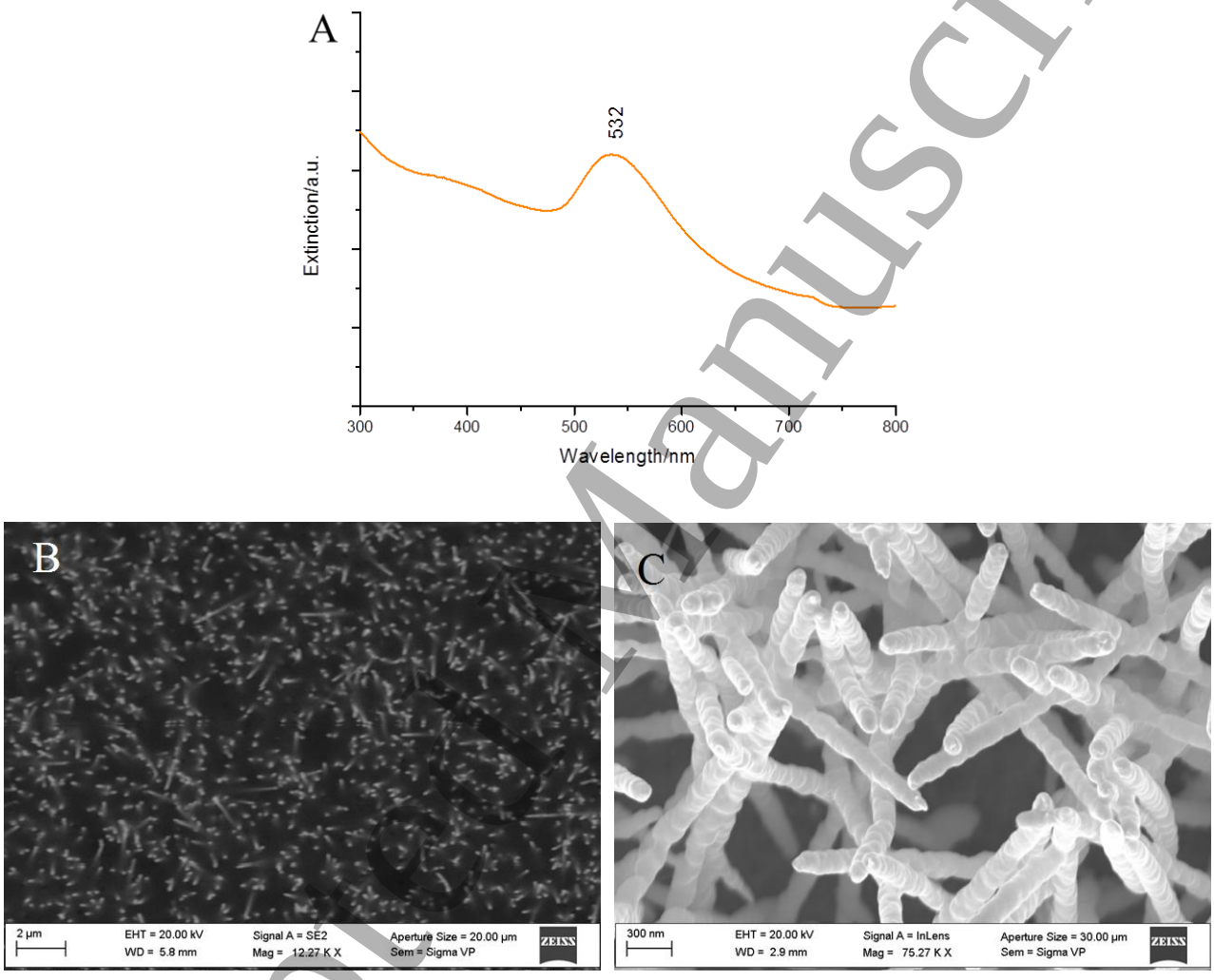

Figure 4 A) UV-Vis-NIR extinction spectrum of AuNWs with 80 nm nominal diameter, dispersed in dichloromethane; FE-SEM images of AuNWs after the B) peeling of one outer face of the membrane from superficial gold and C) after the total etching of polycarbonate membrane in dichloromethane and by cold plasma.

3.3 Preparation and FE-SEM characterization of AgNSs@AuNWs hierarchical structures

Cysteamine is used as bridging ligand suitable to bind the silver nanoparticles onto the gold nanowires. Indeed, the sulfhydryl group of the thiol has a great affinity for gold while the amine group binds silver. Note that an excess of cysteamine is used in order to prevent the possibility that both the sulfhydryl and the amine groups of the same molecules could bind only the AuNW surface, so that a compact cysteamine monolayer is obtained with the amine functionalities protruding out of the Au surface [38,39]. Figure 5 reports the FE-SEM analyses performed after treating the ensemble of AuNWs with cysteamine and AgNSs as described in the experimental section. These images show the presence of the AgNSs bound onto the surface of the AuNWs, in part dispersed and isolated and in part as clusters of nanostars. The latter areas are the spots on which the laser beam used for SERS measurements was preferentially focused.

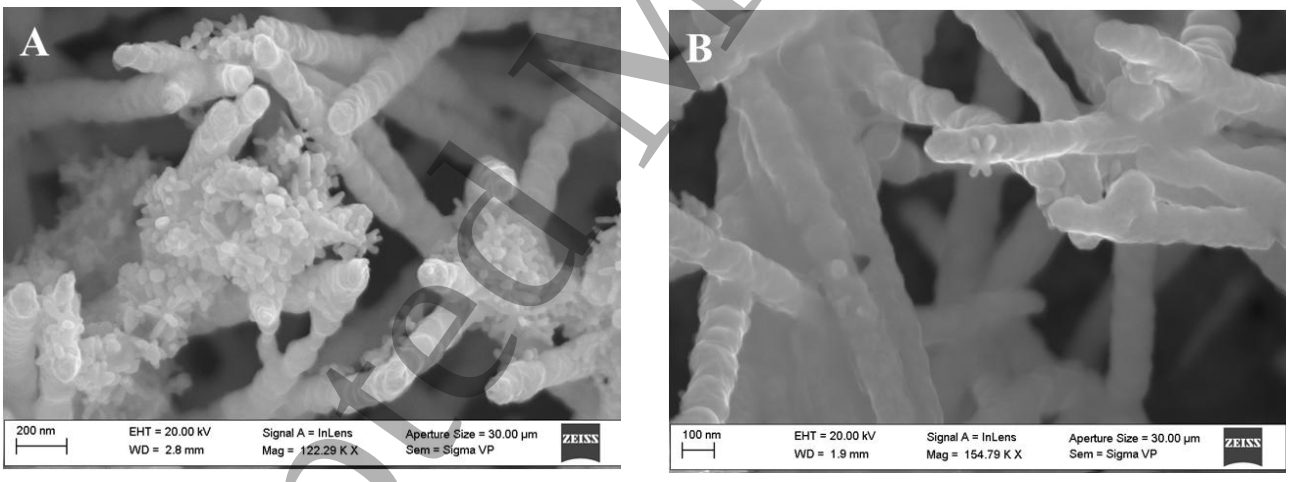

Figure 5 A-B) FE-SEM image of total etched AuNWs bound to AgNSs by means of cysteamine.

3.4 SERS characterization with benzenethiol as Raman probe

The efficiency of several SERS substrates was assessed by employing benzenethiol as reference Raman-probe [12,53-55], whose Raman bands are well known from the literature (see Table S1 in

SM for detailed information). Figure 6 presents the spectra obtained on ensembles of totally etched AuNWs, without or with AgNPs or AgNSs. On the partially etched AuNWs, BT cannot be detected (data not shown), while on totally etched AuNWs the typical Raman spectrum of this BT probe is clearly revealed. This indicates that AuNWs, fully free from the polycarbonate, already act as good SERS substrate. Signals with similar intensity are detected when the nanowire array is decorated with quasi-spherical Ag nanoparticles (i.e. AgNP@AuNW). On the contrary, Figure 6 indicates that a dramatic enhancement in SERS signals is observed when BT is absorbed onto the AgNSs@AuNW hierarchical nanostructures.

These evidences clearly indicate the superior SERS performances of AgNSs when assembled over AuNWs.

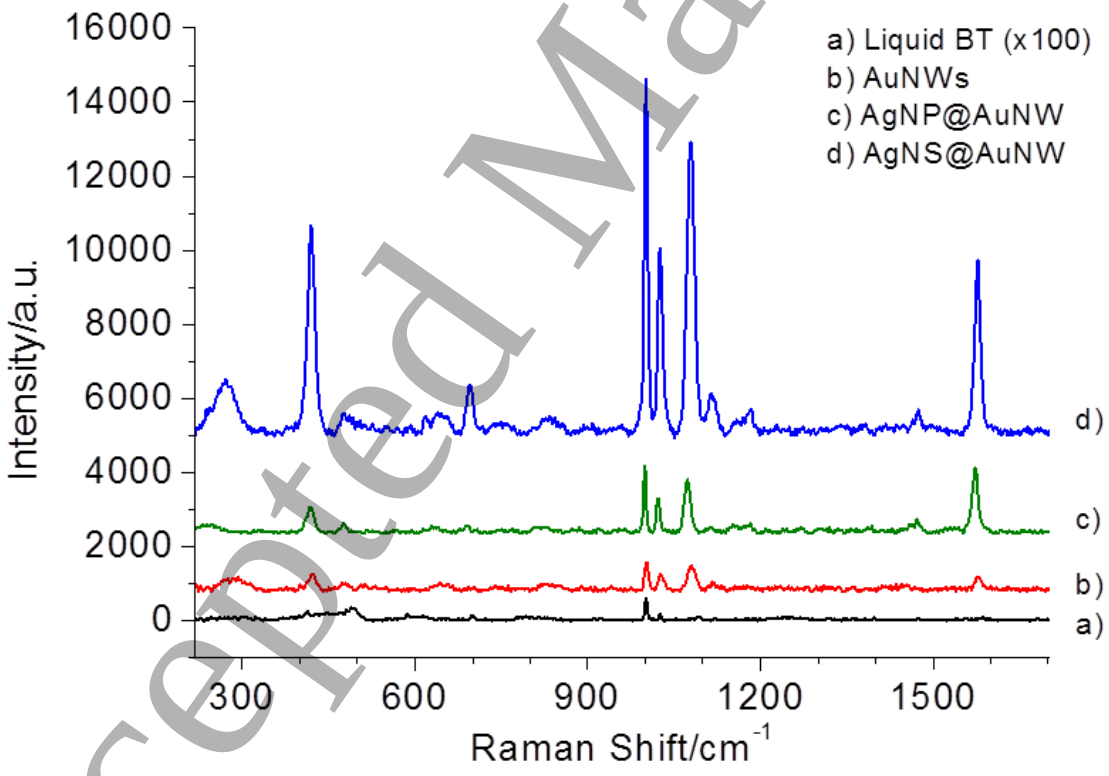

Figure 6 a) Raman spectrum of benezenthiol obtained as pure solution; SERS spectra of a 10^{-5} M BT solution adsorbed on b) totally etched AuNWs, c) totally etched AuNWs + AgNPs

(AgNP@AuNW) and d) totally etched AuNWs + AgNSs (AgNS@AuNW). Spectra acquired with 785 nm excitation and normalized in laser power and acquisition time.

In order to quantify this effect, SERS enhancement factors (EFs) are calculated from the spectra collected on different SERS substrates [56-58]. The number of Raman probe molecules adsorbed by the nanostructures here studied can indeed be very different, depending on the number and dimension of nanomaterial used. Therefore, the calculations of the SERS enhancements factors are performed calculating, at first, the approximate surface area of AuNWs, AgNSs, AgNPs an relevant hierarchical structures, using the geometrical and particle density parameters evaluated from FE-SEM and TEM images. Knowing the different surface areas and the laser spot diameter, taking into account that the benzenethiol molecular area is $0.22nm^2$ [58], by using equation (S1) in SM [59], it is possible to estimate the EF values. The Raman spectrum of pure BT liquid is employed as non-SERS reference. A detailed description about the calculation is presented in the SM section and all parameters and results are resumed in Table S3. The surface selection rules of SERS may results in different enhancements due to the different orientation of the molecules within hot spots [57]. For this reason, two different bands of BT were used for the calculations, at about 1000 and 1025 cm^{-1}, and band integrals were used instead of band height in order to overcome little band shifts found through different substrates. The calculated EF, for the 1025 cm^{-1} band, are in the order of AgNSs@AuNWs ($6.22 \cdot 10^5$), AgNPs@AuNWs ($1.24 \cdot 10^5$) and AuNWs ($9.75 \cdot 10^4$). These esteems are coherent with the experimental results and give a significant indication from the analytical point of view about the efficiency of the tested SERS substrates. It is important to underline that EFs are average values and they take into account the adsorbed molecules whose Raman effects experience a strong enhancement, especially in the so called hot spots.

3.5 Boundary Element Method simulations

Complex morphology of the hierarchical nanostructure above described can be a source of uncertainty when performing the quantitative evaluation of the exposed surface area so preventing the precise calculation of the surface concentration of the Raman probe, necessary for the precise evaluation of SERS enhancement factors from experimental spectra. To overcome the limit of the relative evaluation achieved by comparing SR values, we chose to model and compare the localized intensity of electromagnetic fields in the nanostructures by numerical calculations performed using the boundary element method (BEM). The BEM approach assumes a dielectric environment where bodies with homogeneous and isotropic dielectric functions are separated by abrupt interfaces. It can be employed in the field of plasmonics, in which metallic nanoparticles are embedded in a dielectric background. It presents the advantage that only the boundaries between the different dielectric materials have to be discretized and not the entire volume, performing faster simulations with low memory requirements [40,41].

Figure 7 shows in an arbitrary color scale the SERS enhancement factors (EF) obtained by BEM for AgNS (Fig. 7-A), AuNW (Fig. 7-B) and the coupling of the two nanostructures in AgNS@AuNW (Fig. 7-C), using an excitation source at λ= 785 nm. The EFs are calculated as the forth power of the local fields calculated at the surface of the simulated structures, given unitary the intensity of the exciting electromagnetic field. The enhancements calculated in the AgNS hot spots are of the order of 10^4, but only in very tiny areas, whereas the one obtained for AuNW is order of magnitude smaller (10^2). This shows that the expected enhancements for isolated AgNS and AuNW are small, in particular for the latter. Calculations for the assembled AgNS@AuNW show, on the other hand, that the enhancements increases to a range of 10^5, moreover, in extended areas. The absence of sharp tips, or edges, in both AgNS and AuNW avoid the local fields to concentrate in single nanostructures alone. One can conclude, therefore, that the hierarchical system composed by these two nanomaterials optimizes the enhancement by creating hot spots on large areas due to the proximity of the two. The BEM methodology has been applied also to spherical AgNPs bound to AuNWs in the hierarchical structure AgNP@AuNW. The maximum enhancement (see Fig. 7-D) is

in the order of 10^4 and confined in very limited areas. Comparison between Figure 7-C and 7-D clearly indicates a significantly larger number of hot spots for AgNS@AuNW. The results of the BEM simulations confirm what observed experimentally that is the combination of AgNSs with AuNWs acts synergistically in producing a larger number of hot spots with higher SERS enhancement then for the case of AgNSs, AuNWs or AgNP@AuNW structures.

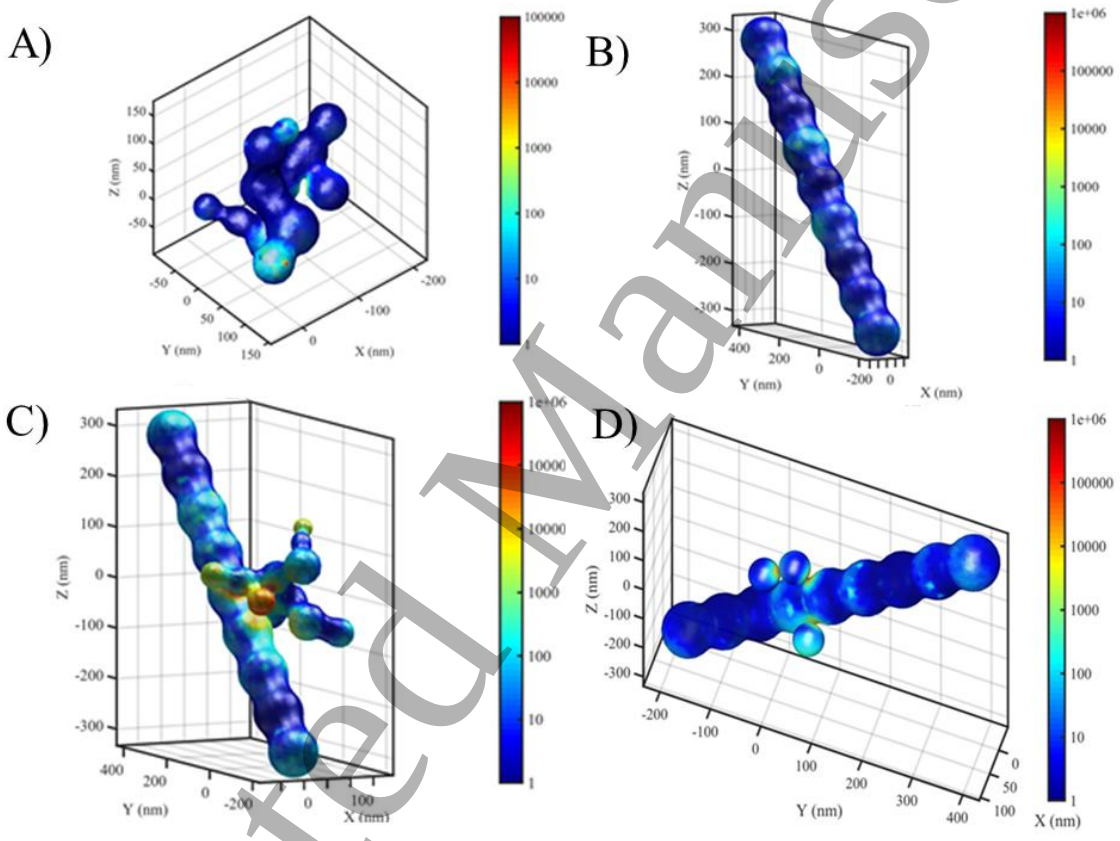

Figure 7 Visual and numerical summary of the results of BEM calculations of the SERS enhancement, produced by an excitation source at λ = 785 nm, on: A) AgNS; B) AuNW;c) AgNS@ AuNW; D) AgNP@AuNW.

Conclusions

The results here presented fully confirm the expectation that binding together anisotropic nanostars with high aspect ratio nanowires acts synergistically to obtain nanonostructures able to produce important SERS enhancement, in excess to 10^5. Interestingly, these enhancements are significantly more relevant than those ~~which~~ characterizing the individual components (i.e. AgNSs and AuNWs) ~~which compose~~ of the final hierarchical nanostructures. It should be emphasized that, in the present study, the high SERS enhamcements that characterize the AgNS@AuNW nanostructures were verified both experimentally and by ~~digital~~ model calculations ~~simulations~~. In particular, BEM calculations put in evidence that the AgNS@AuNW hierarchical structure not only is characterized by an enhancement factor of the order of 10^5, but also presents a high number of hot spots, making possible the detection of analytes in low concentration, ~~such as 10^{-5} M BT in the present work~~. Although the decoration of AuNWs is not even, the obtained results represent a clear proof-of-concept confirming the SERS effectiveness of the AgNS@ AuNW combination. Efforts in obtaining more even decoration are in progress.

Acknowledgements

LL and MM acknowledge the program of the University of Padova P-DiSC #04BIRD2016-UNIPD. Calculations were supported by Cloud.Veneto (http://www.cloudveneto.it) and by the Computational facilities at the Chemical Sciences Department of the University of Padova.

References

[1] Fleischmann M, Hendra P J and McQuillan A J 1974 Chem. Phys. Lett. **26 (2)** 163

[2] Aroca R F, Vallete M C, García Ramos J V, Sánchez-Cortés S, Sánchez Gil J A and Sevilla P, 2014, ed. CSIC (Madrid)

[3] Litti L, Rivato N, Fracasso G, Bontempi P, Nicolato E, Marzola P, Venzo A, Colombatti M, Gobbo M and Meneghetti M 2018 Nanoscale **10** 1272

[4] Litti L and Meneghetti M 2019 Phys. Chem. Chem. Phys. **21** 15515

[5] Park S, Lee J and Ko H 2017 ACS Appl. Mater. Inter. **17** 44088

[6] Zhao Y, Li X, Liu Y, Zhang L, Wang F and Lu Y 2017 Sens. Actuators B **247** 850

[7] González-Domínguez J M, Colusso A, Litti L, Ostric A, Meneghetti M and Da Ros T 2019 ChemPlusChem **84** 862

[8] Shao L, Susha A S, Cheung L S, Sau T K, Rogach A L and Wang J 2012 Langmuir **28** 8979

[9] Khoury C G and Vo-Dinh T 2008 J. Phys. Chem. C **112** 18849

[10] Tognalli N G, Fainstein A, Calvo E J, Abdelsalam M and Bartlett P N 2012 J. Phys. Chem. C **116** 3414

[11] Celiktas A, Ghanem M A and Bartlett P N 2012 J. Electroanal. Chem. **670** 42

[12] Zamuner M, Talaga D, Deiss F, Guieu V, Kuhn A, Ugo P and Sojic N 2009 Adv. Funct. Mater. **19 (44)** 3129

[13] Kim J H, Kang T, Yoo S M, Lee S Y, Kim B and Choi Y K 2009 Nanotechnology **20** 235302

[14] Roy S, Ajmal S M, Baik S and Kim J 2018 Nanotechnology **28** 465705

[15] Guerrero-Martínez A, Barbosa S, Pastoriza-Santos I and Liz-Marzán L M 2011 Curr. Opin. Colloid Interface Sci. **16** 118

[16] Litti L, Reguera J, García de Abajo F J, Meneghetti M and Lis-Marzán L M 2020 Nanoscale Horiz. **5** 102

[17] Wang Y, Camargo P H C, Skrabalak S E, Gu H and Xia Y 2008 Langmuir **24** 12042

[18] García-Leis A, García-Ramos J V and Sánchez-Cortés S 2013 J. Phys. Chem. C **117** 7791

[19] Kumar P S, Pastoriza-Santos I, Rodriguez-Gonzales B, García de Abajo F J and Luis-Marzán L M 2007 Nanotechnology **19** 015606

[20] Tsoulos T V and Fabris L 2018 J. Phys. Chem. C **122** 28949

[21] Tang H, Meng G, Huang Q, Zhang Z, Huang Z and Zhu C 2012 Adv. Funct. Mater. **22** 218

[22] Kwan K and Yoon J K 2005 J. Phys. Chem. B **109 (44)** 20731

[23] Kwan K and Lee H S 2005 J. Phys. Chem. B **109 (40)** 18929

[24] Zhang Q, Lee Y H, Phang I Y, Lee C K and Ling X Y 2014 Small **10 (31)** 2703

[25] Fu C Y, Kho K W, Dinish U S, Kohe Z Y and Malini O 2012 J. Raman Spectrosc. **43** 977

[26] Zhao L, Blackburn J and Brosseau C L 2015 Anal. Chem. **87** 441

[27] Orendorff C J, Gearheart L, Jana N R and Murphy C J 2006 J. Phys Chem. C **8** 165

[28] Mahmoud M A and El-Sayed 2013 J. Phys Chem. Lett. **4** 1541

[29] Kurniawan A and Wang M-J 2017 Nanotechnology **28** 355703

[30] Yoon I, Kang T, Choi W, Kim J, Yoo Y, Joo S-W, Park Q-H, Ihee H and Kim B 2009 J. Am. Chem. Soc. **131** 758

[31] Lee S J, Baik J M and Moskovits M 2008 Nano Lett. **8** 3244

[32] Camargo J H K, Cobley C M, Rycenga M and Xia J 2009 Nanotechnology **20** 434020

[33] Kurniawan A and Wang M-J 2017 Nanotechnology **28** 355703

[34] Ankudze B and Pakkanen T T 2018 Appl. Surf. Sci. **453** 341

[35] Sanguansap Y, Karn-orachai K and Laocharoensuk R 2020 Appl. Surf. Sci. **500** 144049

[36] Scopece P, Baker L, Ugo P and Martin C R, 2006 Nanotechnology **17** 3951

[37] Moretto L M, Tormen M, De Leo M, Carpentiero and Ugo P 2011 Nanotechnology **22** 185305

[38] Shein J B, Lai L M H, Eggers P K, Paddon-Row M N and Gooding J J 2009 Langmuir **25** 11121

[39] Silvestrini M and Ugo P 2013 Anal. Bioanal. Chem. **405** 995

[40] Hohenester U and Trügler A 2012 Comput. Phys. Commun. **183** 370

[41] Hohenester U Comput. 2018 Phys. Commun. **222** 209

[42] Lee P C and Meisel D J 1982 J. Phys. Chem. **86** 3391

[43] Cañamares M V, García-Ramos J V, Gomez-Varga J D, Domingo C and Sánchez-Cortés S 2005 Langmuir **21** 8546

[44] Menon V P and Martin C R 1982 Anal. Chem. **63** 1920

[45] De Leo M, Kuhn A and Ugo P 2007 Electroanalysis **19 (2-3)** 227

[46] De Leo M, Pereira F C, Moretto L M, Scopece P, Polizzi S and Ugo P 2007 Chem. Mater. **19 (24)**

[47] Yu S, Li N, Wharton J, Martin C R 2003 Nano Lett. **3 (6)** 815

[48] Stortini A M, Fabris S, Saorin G, Verga Falzacappa E, Moretto L M and Ugo P 2019 Nanomaterials **9** 1

[49] Esteban R, Borisov A G, Nordlander P and Aizpurua J 2012 Nat. Commun. **3** 825

[50] Caswell K K, Bendu C M and Murphy C J 2003 Nano Lett. **3** 667

[51] Cho T J and Hackley V A 2010 Anal. Bioanal. Chem. **398** 2003

[52] Pereira F C, Boldrin-Zanoni M V, Moretto L M and Ugo P 2007 Quim. Nova**30 (7)** 1550

[53] McFarland A D, Young M A, Dieringer J A and Van Duyne R P 2005 J. Phys. Chem. B **109** 11279

[54] Valley N, Greeneltch N, Van Duyne R P and Schatz G C 2013 J. Phys. Chem. Lett. **4** 2599

[55] Fontana J, Livenerec J, Bezaresd F J, Caldwell J D, Rendell R and Ratna B R 2013 Appl. Phys. Lett. **102** 20160

[56] Cintra S, Abdelsalam M E, Bartlett P N, Baumberg J J, Kelf T A , Sugawarab Y and Russell A E 2006 Faraday Discuss. **132** 191

[57] Le Ru E C, Blackie E, Meyer M and Etchegoin P G 2007 J. Phys. Chem. C **111** 13794

[58] Guieu V, Lagugne-Labarthet F, Servant L, Talaga D and Sojic N 2008 Small **4 (1)** 96

[59] Le Ru E C, Blackie E, Meyer M and Etchegoin P G 2007 J. Phys. Chem. C **111** 13794